



ORIGINAL ARTICLE

Catalytic conversion of greenhouse gases (CO₂ and CH₄) to syngas over Ni-based catalyst: Effects of Ce-La promoters

Ahmad Salam Farooqi^{a,b}, Basem M. Al-Swai^a, Farida Hamimi Ruslan^a,
Noor Asmawati Mohd Zabidi^c, R. Saidur^{d,e}, Syed Anuar Faua'ad Syed Muhammad^f,
Bawadi Abdullah^{a,g,*}

^a Chemical Engineering Department, Universiti Teknologi PETRONAS, 32610 Seri Iskandar, Malaysia

^b Department of Chemical Engineering, Wah Engineering College, University of Wah, Wah Cantt, 47040 Punjab, Pakistan

^c Fundamental and Applied Sciences Department, Universiti Teknologi PETRONAS, 32610 Seri Iskandar, Malaysia

^d Research Centre for Nano-Materials and Energy Technology (RCNMET), School of Science and Technology, Sunway University, Jalan University, 47500 Bandar Sunway, Selangor Darul Ehsan, Malaysia

^e Department of Engineering, Lancaster University, Lancaster LA1 4WY, UK

^f School of Chemical and Energy Engineering, Faculty of Engineering, Universiti Teknologi Malaysia, UTM Skudai, 81310 Skudai, Johor, Malaysia

^g Centre of Contaminant Control and Utilization (CenCoU), Institute of Contaminant Management for Oil and Gas, Universiti Teknologi PETRONAS, 32610 Seri Iskandar, Malaysia

Received 10 February 2020; revised 11 April 2020; accepted 12 April 2020

Available online 19 April 2020

KEYWORDS

Syngas;
Reforming;
Catalyst;
Greenhouse gases;
Promoters

Abstract Dry reforming of methane (DRM) is an emerging technology as it can simultaneously serve as a prospective alternative energy source and mitigate greenhouse gases (e.g. CH₄ and CO₂). However, the industrial applications of DRM remain restricted due to the poor prospect of catalyst deactivation. In this study, the effects of adding CeO₂ and La₂O₃ as promoters on the catalytic performance of Ni/Al₂O₃ catalyst were assessed. Catalysts such as Ni/Al₂O₃, Ni/Al₂O₃-La₂O₃, and Ni/Al₂O₃-CeO₂ were synthesized at nano level using the sol-gel method. Citric acid was added to improve the reactivity of catalysts before the application of DRM. Various characterisation techniques were used to characterise synthesized catalysts, including Brunauer-Emmett-Teller (BET) analysis, temperature-programmed reduction (TPR), field emission scanning microscopy (FESEM), X-ray diffraction (XRD), and transmission electron microscopy (TEM). The

* Corresponding author at: Chemical Engineering Department, Universiti Teknologi PETRONAS, 32610 Seri Iskandar, Malaysia.

E-mail addresses: bawadi_abdullah@utp.edu.my, bawadi73@gmail.com (B. Abdullah).

Peer review under responsibility of King Saud University.



Production and hosting by Elsevier

results revealed that the BET surface area of the synthesized catalyst slightly decreased when CeO₂ and La₂O₃ were added due to the deposition on the porous structure of the support. Meanwhile, the XRD results demonstrated the increase in reducibility and dispersion of Ni using CeO₂ promoter and the inhibited development of the non-active phase of Ni/Al₂O₃ using La₂O₃ promoter (i.e. NiAl₂O₄), resulting in the carbon formation and reduced efficiency of the catalyst. The catalytic performance in DRM at 800 °C showed that Ni/Al₂O₃-CeO₂ catalyst exhibited higher catalytic performance in terms of CH₄ and CO₂ conversion with 89.6% and 91.2% respectively. While Ni/Al₂O₃-La₂O₃ was found to play a substantial role in the stability of the chemical reaction during the 8 h reaction time-on-stream.

© 2020 The Author(s). Published by Elsevier B.V. on behalf of King Saud University. This is an open access article under the CC BY-NC-ND license (<http://creativecommons.org/licenses/by-nc-nd/4.0/>).

1. Introduction

An increase of 30% in the global consumption of energy is expected by 2040 (Kargbo et al., 2010). Although renewable (e.g. solar and wind) and alternative (e.g. hydrogen cell) energy resources have recently become popular, fossil fuels like natural gas, oil, and coal still play a substantial role in meeting the global energy demands. The energy generation from fossil fuels release a significant amount of greenhouse gases (GHGs), which mainly comprise of carbon dioxide (CO₂) and methane (CH₄); thus, contributing to global warming and other adverse environmental changes (Mozammel, 2017; Oyama et al., 2012). There have been numerous attempts to minimise the emission of CO₂ and CH₄ in order to prevent global warming. The transformation of methane gas into synthesis gas (a mixture of H₂ and CO) that can be conveniently processed to produce chemicals and fuels is one of the significant means to address these environmental issues (Djinović et al., 2012; Tao et al., 2014; Xu et al., 2009a; Zhao et al., 2017).

Accordingly, the composition of synthesis gas largely depends on the synthesis process and the composition of the raw materials. The syngas can be formed from a range of main fossil fuels, such as coal, petroleum coke, and natural gas (Abdullah et al., 2017; Ghoneim et al., 2016). However, the cheapest and most environmentally friendly methods to produce syngas are typically based on natural gas (Ghoneim et al., 2016; Fayaz et al., 2016). The reforming process is one of the most familiar methods used at the industrial scale to produce syngas, such as (1) partial oxidation of methane (POM), (2) dry reforming of methane (DRM), and (3) steam reforming of methane (SRM) (Jang et al., 2013). Among these three reforming processes, the catalytic SRM reaction is the most prevalent and conventional route to produce syngas (De Freitas Silva et al., 2013; Kim et al., 2015; Nieva et al., 2014; Wu et al., 2013). However, the main setbacks of this process include a higher ratio of H₂ and CO (i.e. > 3) and a large amount of undesirable production of CO₂. Additionally, SRM requires intensive energy input due to its endothermic reaction and exorbitant in nature (Guo et al., 2004). Meanwhile, POM can generate syngas when the ratio between H₂ and CO equals to 2 but the existence of hot areas and excessive reactivity make the handling process not easy (Xu et al., 2013). In addition, DRM has the capacity to handle two types of GHGs, specifically CO₂ and CH₄, for syngas production. The advantage of DRM for syngas production lies ideally in one molar ratio of H₂ and CO, which is beneficial for the

Fischer-Tropsch process (Guo et al., 2004; Wang et al., 1996, 2018b).

The utilisation of a catalyst is vital during the reforming process of CH₄ for complete conversion of the reactants. Numerous past studies focused on improving the catalytic performance, such as the activity and stability of a catalyst, to support the DRM process. Nearly all such practices focus on overcoming the catalyst deactivation problem. The primary reason for the catalyst deactivation problem lies in the occurrence of coke deposition because, at higher temperature of reaction (Bartholomew, 2001; Zhang et al., 1996), the carbon formed covers the active sites of the catalyst (Abd Ghani et al., 2019; Siang et al., 2018b). Non-noble metals such as nickel- and cobalt-based catalysts have been widely used for the DRM reaction due to their high selectivity, catalytic activity, and low carbon formation (Al-Swai et al., 2019; Bian et al., 2017; Bradford and Vannice, 1999; Selvarajah et al., 2016; Siang et al., 2018a; Stroud et al., 2018; Xu et al., 2009b). Hence, numerous efforts have been made to acquire improved synthesis and design of stable Ni-based catalyst with high carbon resistance. One of the effective and practical strategy to overcome catalyst deactivation is utilizing nickel with the addition of support having strong Lewis basicity such as La₂O₃, CaO, and MgO (Al-Swai et al., 2019; Usman et al., 2015).

Al₂O₃ is the most suitable support for the most catalytic materials. But due to the acidic nature of Al₂O₃, it enhances the coke deposition which effects the catalyst deactivation (Wang et al., 2018a). Mo-promoted Ni/Al₂O₃ catalyst for DRM caused a considerable reduction in the catalytic activity compared to the non-promoted Ni/Al₂O₃ catalyst that showed high catalytic activity as reported by (Yao et al., 2017). This was primarily due to set up of a distinct Ni⁰ phase that disconnected from Mo and hence decreased the overall basicity of the catalyst. Meanwhile, the addition of La₂O₃ into Ni-Al catalyst can be beneficial as it inhibits the coke formation during the reaction of DRM and reduces the support acidity, which favour the chemisorption and dissociation of carbon dioxide and eliminate carbon via reverse Boudouard reaction (Al-Fatesh et al., 2014). Furthermore, the dispersion of La₂O₃ over Al₂O₃ and Ni crystallites prevents the growth of Ni grains at higher temperature, which minimises the sintering of catalyst due to the formation of La₂O₂CO₃ (Charisiou et al., 2019). On the other hand, Ceria exhibits the characteristics of releasing and storing oxygen. As a result, the reduction of Ce⁴⁺ to Ce³⁺ leads to the formation of oxygen vacancies (Yao et al., 2018). The release of oxygen occurs in oxygen-poor medium

whereas re-oxidation occurs in oxygen-rich medium (Xu et al., 1999). The effects of adding ceria (CeO₂) doped with Pr, Zr and Nb to Pt/Al₂O₃ catalyst were evaluated by (da Fonseca et al., 2020) and found that there was a substantial increase in catalytic activity on doping the catalyst. The Pr exhibited maximum reducibility of ceria (23%) and Pt/CePr/Al₂O₃ displayed the paramount activity and stability. (Luissetto et al., 2015) studied the DRM reaction using different supports, specifically CeO₂, MgO, and mixed oxide CeO₂-MgO, on Ni/Al₂O₃ catalyst and proposed a lower temperature of reaction for improved Ni distribution.

In view of the above, finding a new catalyst that can resist the deposition of carbon using suitable support and promoter is vital in DRM. In the present study, the effects of Ce and La promoters on the physiochemical properties of Ni/Al₂O₃ catalysts, synthesized using the sol-gel method, were compared. The catalysts were characterized to describe the effects of Ce and La promoters on the catalyst performance.

2. Materials and methods

2.1. Materials

For the preparation of catalysts in the present study, Ni (NO₃)₂·6H₂O served as the source of an active metal and Al (NO₃)₃·9H₂O served as the source of catalyst support. In addition, La (NO₃)₃·6H₂O and Ce (NO₃)₃·6H₂O were utilised as catalyst promoters. Besides that, citric acid was utilised as the chelating agent. The gases for the reduction method before the reaction were H₂ and N₂, while CH₄, CO₂, and N₂ were utilised during the test reaction.

2.2. Nano-catalyst synthesis

The sol-gel method was applied to produce Ni-based catalysts. There were various materials and reaction conditions involved. Typically, the stoichiometric amount of active metal, support, promoters, and citric acid were first mixed and dissolved in DI water. Ammonium hydroxide solution (28 vol.%) was added dropwise with continuous stirring to adjust the pH around 9–9.5. Following that, the solution was heated on the warm plate at 80 °C and continuously stirred for 6 h until the gel was formed. The gel was subsequently placed in an oven at 393 K for 12 h before it was calcined in static air for 5 h at 900 °C. The produced catalysts Ni/Al₂O₃, Ni/Al₂O₃-CeO₂, Ni/Al₂O₃-La₂O₃ were denoted as CAT-1, CAT-2 and CAT-3 respectively and their weight composition are presented in Table 1. As shown in the table, the nickel loading was 10 wt % whereas CeO₂ and La₂O₃ promoters were 10 wt%.

Table 1 Composition of the prepared catalysts.

Catalyst labelling	Catalyst	Support/Promoter	Composition (wt.%)
CAT-1	Ni/Al ₂ O ₃	Al ₂ O ₃ /NA	Ni: 10%, Al ₂ O ₃ : 90%
CAT-2	Ni/Al ₂ O ₃ -CeO ₂	Al ₂ O ₃ /CeO ₂	Ni: 10%, Al ₂ O ₃ : 80%, CeO ₂ : 10%
CAT-3	Ni/Al ₂ O ₃ -La ₂ O ₃	Al ₂ O ₃ /La ₂ O ₃	Ni: 10%, Al ₂ O ₃ : 80%, La ₂ O ₃ : 10%

2.3. Characterisation of catalyst

Surface area analysis, specifically Brunauer-Emmett-Teller (BET) analysis, was conducted using Micromeritics ASAP 2020 to measure the surface area of catalytic materials (by N₂ adsorption). The specific surface areas and the pore size distribution were calculated using Brunauer-Emmett-Teller (BET) and Barrett-Joyner-Halenda (BJH) methods, respectively. Additionally, the reducibility of the catalysts was studied using Thermo Scientific TPD/R/O (1100). For this study, 50 mg catalyst was heated in a reactor with N₂ flow of 20 mL min⁻¹ at 250 °C for 1 h. After the catalyst was degassed by injecting hydrogen flow (5% in N₂), it was heated from 40 °C to 1000 °C. The basicity of the catalysts was measured using the same equipment of H₂-TPR. Similarly, the materials were pre-heated for 1 h at 500°C, followed by cooling down at 80 °C. For the desorption of CO₂, 10% CO₂/He was injected for 1 h. Following that, pure N₂ was injected to desorb CO₂ for 15 min. The CO₂ desorption was recorded while the samples were further heated to 800 °C at a constant rate of 10 °C min⁻¹. Besides that, field emission scanning electron microscopy (FESEM) analysis was conducted using Zeiss Supra55 VP to obtain the topography of the surface of catalyst. Its topography provides information about the surface features in terms of surface irregularities and the size, shape, and distribution of particles and the elemental composition and internal structure of the catalyst. Apart from that, the XRD technique was applied in this study to characterise the calcined mixed oxide catalysts. Advance X-ray diffractometer (Bruker D8B) with a range of between 10° and 90° and step size of 0.04° per step was utilised. Phases existing in the samples were identified by comparison with reference patterns in the ICDD database.

2.4. Experimental setup of DRM

The DRM reaction was recorded in a tube furnace-based reactor according to specific procedures. In particular, a 20 mg catalyst sample, which was sandwiched between quartz wool layers, was placed in the tube reactor. The bed was then positioned at the desired location within the reactor. Following that, N₂ gas was injected at flow rate of 20 mL min⁻¹ for 30 min to evacuate any air in the reactor. As the temperature was increased up to 800 °C, a mixture of H₂/N₂ gas was injected at a rate of 30/30 mL min⁻¹. The reduction was carried out for 1 h to activate the catalyst. Subsequently, in order to remove H₂ from the reactor, it was purged again for 15 min with a flow rate of 20 mL min⁻¹. At the same time, the temperature was reduced to 650 °C and increased to 800 °C for 15 min. Once the temperature recorded 800 °C, N₂, CO₂, and CH₄ gases were purged into the reactor at a ratio of 1:1:1 for about 8 h with a flow rate 60 mL min⁻¹. Meanwhile, the volume fraction of the product stream was processed using an online gas chromatograph (GC). The percentage of reactant conversions, X_i (i denotes CH₄ and CO₂), and the syngas ratio (H₂:CO) were estimated based on the following equations:

$$X_i (\%) = \frac{Q_i^{In} - Q_i^{Out}}{Q_i^{In}} \times 100 \quad (1)$$

$$H_2/CO = \frac{Q_{H_2}^{Out}}{Q_{CO}^{Out}} \times 100 \quad (2)$$

3. Results and discussion

3.1. Textural properties

Table 2 presents the BET surface area of the prepared catalysts. Overall, CAT-1 (the catalyst without any promoter) recorded the highest BET surface area measured due to its alumina trait. An area of 134.1 m² g⁻¹ was recorded. Besides that, the BET surface area decreased when CeO₂ and La₂O₃ promoters were introduced, with the values of 126.9 m² g⁻¹ and 123.6 m² g⁻¹, respectively. The decrease in the BET surface area can be explained by the addition of CeO₂ and La₂O₃ that cover alumina pores (De Freitas Silva et al., 2013). Moreover, there was a small difference in the BET values with the addition of promoters. Likewise, CAT-1 also recorded the highest average pore size (8.5 nm) and pore volume (0.27 cm³/g). However, these values decreased with the addition of CeO₂ and La₂O₃ promoters due to the blockages of the pores.

Fig. 1(a) shows the isotherms of the N₂ adsorption-desorption associated with the catalysts 1 (a), they are characterized as of group IV isotherm that represents materials of mesoporous (2–50 nm) characteristics, which are in accordance to IUPAC (Donohue and Aranovich, 1998). Moreover, the adsorption/desorption hysteresis loops took place within the range of P/P₀, 0.60–0.90 and belong to H1 hysteresis loop. In other words, the catalysts contain highly uniform mesoporous channels and have agglomerates of approximately uniform spheres (Donohue and Aranovich, 1998). Referring to Fig. 1(b), the pore size distribution of the synthesized catalysts shows a relatively narrow distribution with the peak values of

around 10 nm for CAT-1 and 8 nm for CAT-2 and CAT-3. With the addition of these promoters, the pore size of the catalysts reduced due to the partial blockage of the pores.

3.2. XRD

Fig. 2 presents the XRD pattern of Ni/Al₂O₃ calcined catalysts with and without promoters. The pattern of the three prepared catalysts was recorded within the scan range of between 10° and 90°. Furthermore, XRD results revealed the presence of Al₂O₃, NiAl₂O₄, and CeO₂ crystalline phases. However, crystalline peaks associated with Ni or NiO were found not visible due to the presence of small Ni particles and high dispersion on the support surface (Le Saché et al., 2018).

Meanwhile, diffraction peaks of alumina, Al₂O₃ (JCPDS 00-010-0339), appeared at (2θ) 37.2°, 45.4°, and 66.4° and corresponded to the respective index of 311, 400, and 440. The peaks due to the NiAl₂O₄ can be seen at 18.9°, 33.3°, 37.2°, 45.5°, 60.3°, 66.4° and 84.4°; however, there was an overlap of that of Alumina peaks and NiAl₂O₄ as reported in a previous study (Le Saché et al., 2018). The coexistence of Al₂O₃ and NiAl₂O₄ phases indicate the inadequacy of 10 wt% Ni to transfer the gamma phase of alumina into NiAl₂O₄ (Penkova et al., 2011). Rahbar Shamskar et al. (2017) showed that NiO peaks were absent because of the strong interaction between NiO and Al₂O₃ which also indicates the high dispersion of NiO. CAT-2 with CeO₂ revealed peaks at (2θ) 28.7°, 33.3°, 47.6°, 56.5° and 88.6° (JCPDS 00-004-0593), which indicate the fluorite structure of Ceria. On the other hand, the diffractogram of CAT-3 with La₂O₃ demonstrated the least

Table 2 Textural properties of the synthesized catalysts.

Catalyst	BET surface area (m ² /g)	Average pore size (nm)	Pore volume (cm ³ /g)	Average crystal size ^a (nm)
CAT-1	134.1	8.5	0.27	4.35
CAT-2	126.9	6.2	0.25	2.41
CAT-3	123.6	6.1	0.22	7.86

^a Debye–Scherrer equation used to evaluate XRD peaks for NiAl₂O₄.

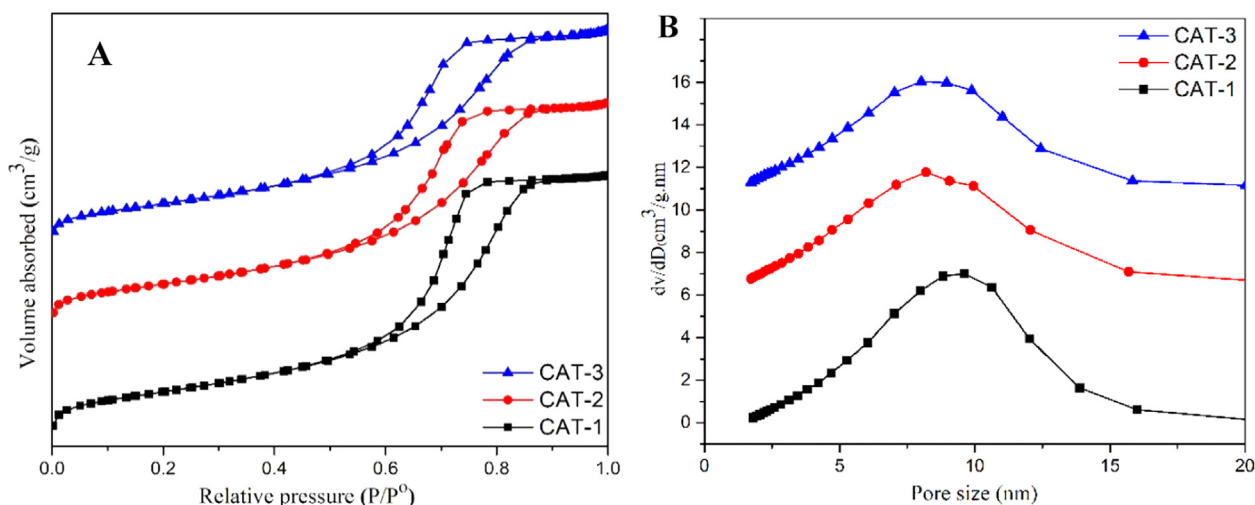


Fig. 1 (a) N₂ adsorption-desorption isotherm curves and (b) pore size distribution of the prepared catalysts.

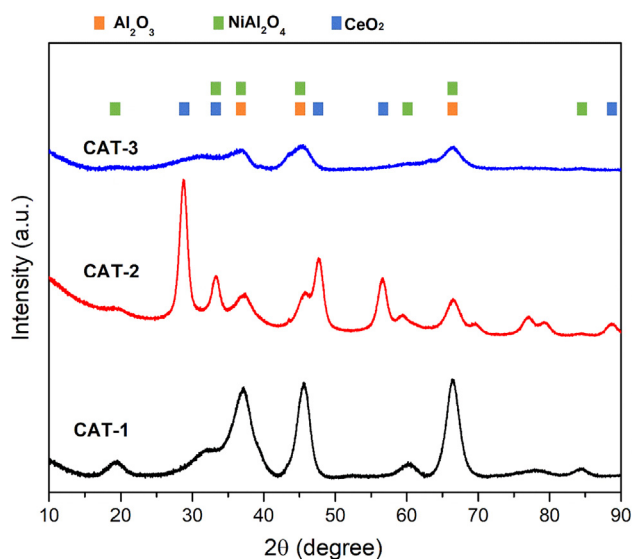


Fig. 2 XRD analysis of calcined samples.

structure crystallinity, which indicates that La_2O_3 is amorphous and has a small reflection at peaks that are the same to that of Al_2O_3 .

Table 2 presents the average crystal sizes of the catalysts that were calculated using the Debye–Scherrer equation. The average crystal size of NiO was estimated using the main peaks of NiAl_2O_4 as it is difficult to determine the crystal size of NiO due to the formation of NiAl_2O_4 spinal structure. The values thus signify CeO_2 in lowering the crystal size of the catalyst, which indicates the higher dispersion of Ni on the surface of support.

3.3. Morphological analysis

As shown in Table 2, CAT-1 demonstrated high irregularity and more porous structure that supports the high surface area of $\text{Ni}/\text{Al}_2\text{O}_3$ catalyst. Meanwhile, CAT-2 demonstrated regular and uniform morphology, which indicate the distribution of Ceria on the surface of catalyst. The presence of CeO_2 appears to obstruct the formation of NiAl_2O_4 and facilitates the dispersion of Ni on the support surface. On the other hand, CAT-3 with La_2O_3 demonstrated some irregular shapes that may be due to the growth of irregular crystalline grains during the synthesis (Aghamohammadi et al., 2017).

Fig. 3 presents the FESEM images and EDX results of the prepared catalysts. In particular, the EDX results reflect the elemental composition of catalysts. The amount of Ni found on the surface of catalyst increased with the addition of

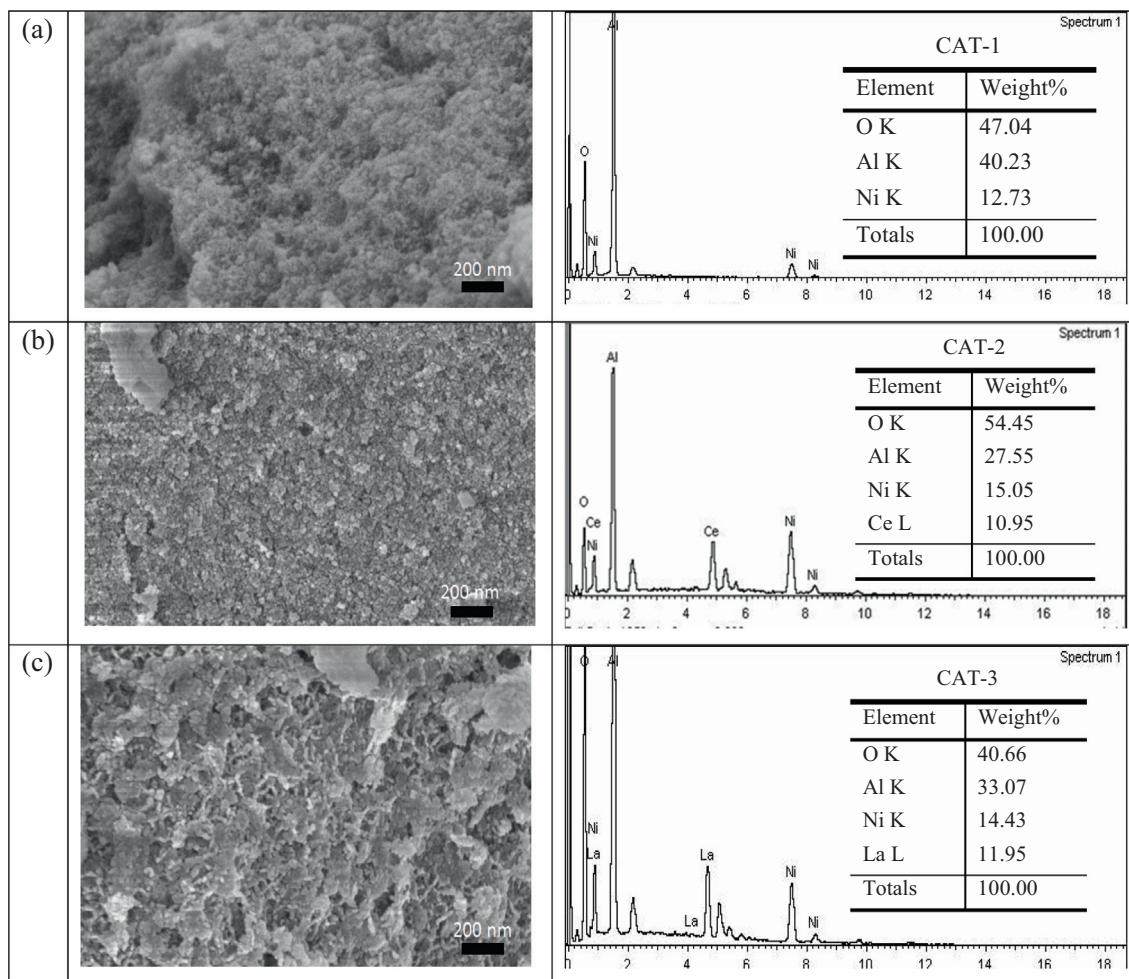


Fig. 3 FESEM images and EDX graphs of pre reaction catalyst at 50.0 K \times magnification.

CeO₂, which shows that Ce facilitates the dispersion of Ni and increases the weight percentage. The value increased from 12.73 wt% (CAT-1) to 15.05 wt% (CAT-2) as CeO₂ was added as a promoter. Similarly, there was an increase of 14.43 wt% (CAT-3) when La₂O₃ was added as a promoter.

3.4. TEM analysis

Fig. 4 shows the transmission electron microscope (TEM) images of the three synthesized catalysts. Two spots were detected—the presence of alumina causes the observed difference and the presence of Ni metal species causes the dark contrast (Kim et al., 2015). In particular, CAT-1 exhibited larger particle size with seemingly round shape particles whereas CAT-2 demonstrated higher dispersion of Ni particles. The clear particle agglomeration in Fig. 4(c) supported the FESEM results in Fig. 3(c).

3.5. H₂-TPR

Fig. 5 presents the TPR plots for the three prepared catalysts, which revealed that NiO was reduced to metallic Ni with obvious peak differences when the temperature achieved below 850 °C. Unlike the case of Ni/Al₂O₃, both promoted catalysts showed higher peaks of hydrogen consumption. CeO₂ and La₂O₃ are structural promoters that limit the aggregation of Ni particles during the reduction of H₂ (Jiang et al., 2003).

Meanwhile, the peaks at lower temperature (300–450 °C) can be attributed to the reduction of Ni that weakly interacts with the support. Referring to the TPR plots, CAT-1 revealed a small peak whereas striking peaks appeared for CAT-2 and

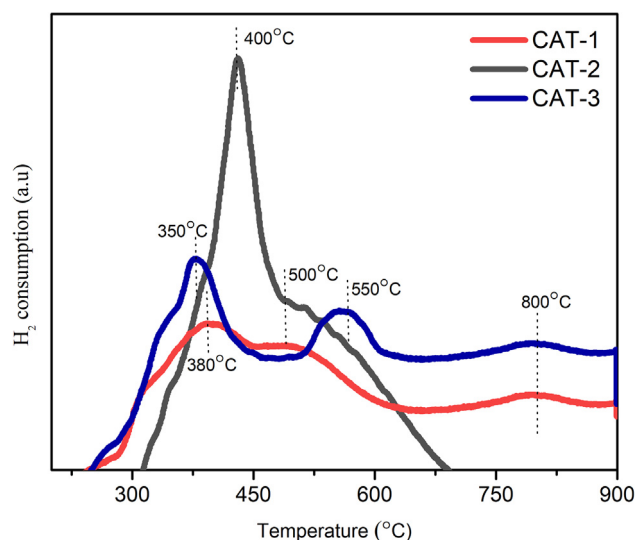


Fig. 5 TPR analysis of calcined samples.

CAT-3 (Farooqi et al., 2020). In other words, CeO₂ and La₂O₃ improved the reduction of Ni.

Besides that, CAT-2 demonstrated the largest reduction peak for NiO at around 400 °C, which suggests that the presence of CeO₂ did facilitate the dispersion of a large fraction of NiO species that are weakly attached to the support. The second peak for both CAT-1 and CAT-2 at 500 °C and CAT-3 at 550 °C can be ascribed to the reduction of Ni that is moderately attached to the support. Furthermore, the peak reduction

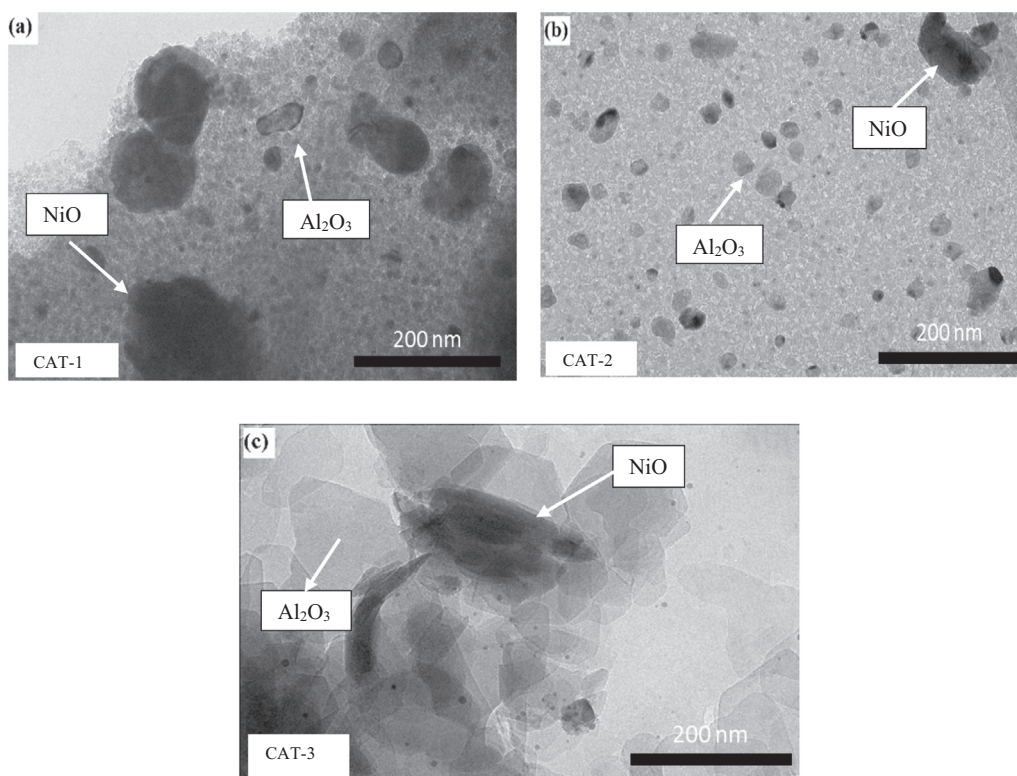


Fig. 4 TEM micrographs of calcined samples.

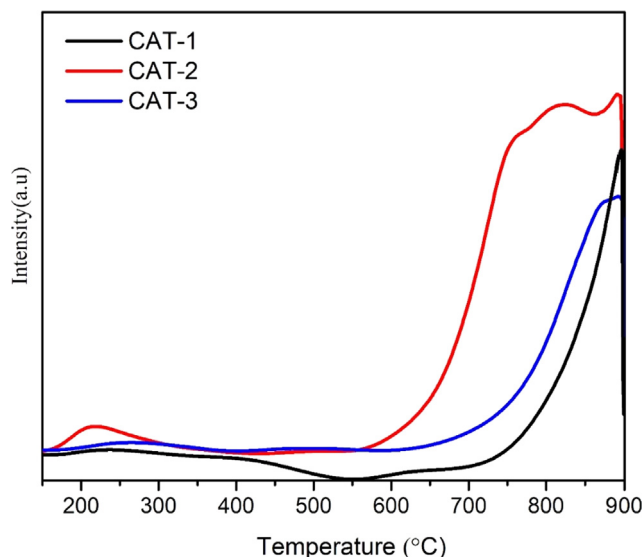


Fig. 6 CO₂-TPD analysis of calcined samples.

appeared to be evident at 800 °C for CAT-1, which corresponded to the reduction of Ni with a strong bond formed between Ni and the support during the formation of Ni/Al₂O₃, (De Freitas Silva et al., 2013).

3.6. CO₂-TPD

The basic sites present locations where the adsorbed CO₂ has been desorbed. Generally, the Lewis alkaline sites are based on the desorption temperature of CO₂: (1) less than 200 °C: weak; (2) between 200 °C and 400 °C: medium; (3) between 400 °C and 600 °C: strong; (4) more than 600 °C: very strong. Fig. 6 presents the CO₂-TPD spectra of catalysts CAT-1, CAT-2, and CAT-3. Overall, the CO₂-TPD profile for all catalysts appeared to be very similar in shape, as the main peak was stretched within the range of between 600 °C and 900 °C.

The first peak at the range of between 150 °C and 300 °C can be attributed to the weakly adsorbed CO₂ on the basic sites of the surface of catalysts. The main peak of the CO₂-TPD profile was centered at 800 °C for CAT-2 and 850 °C for CAT-1, which may be due to desorption of CO₂ that strongly

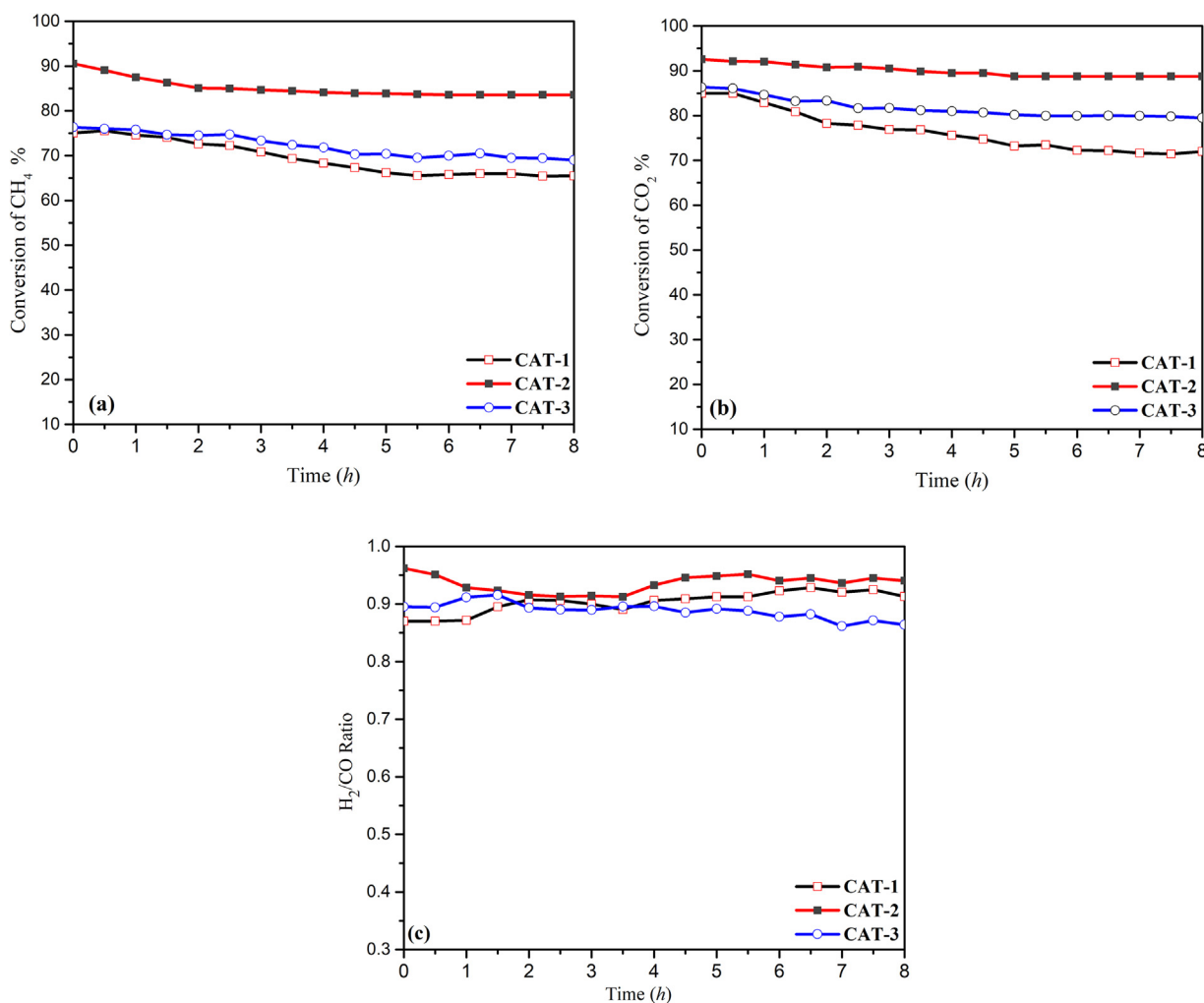


Fig. 7 (a) Conversion of CH₄, (b) Conversion of CO₂ and (c) syngas ratio (H₂/CO) at 800 °C.

attached to the basic sites (Xu et al., 2017). Meanwhile, CO₂ desorption peak appeared to be higher for CAT-2 with CeO₂ which is expected to exhibit strong resistance against deactivation considering that catalysts with higher basic sites can reduce coke formation and prolong the activity of the catalysts (Radlik et al., 2015).

3.7. Catalytic methane dry reforming evaluation

It is well known that the extent of a chemical reaction only depends on the thermodynamics of the reaction, and catalyst could only change the rate of the reaction. Fig. 7 presents the occurrence of DRM reaction at 800 °C for 8 h. The conversion of CH₄ and the perceptible influence of CeO₂ and La₂O₃ on the catalytic performance can be observed in Fig. 7(a). In particular, CAT-1 and CAT-3 recorded the same initial conversion of 75%. The conversion of CH₄ subsequently dropped to 64% after 8 h of reaction. CAT-2 with La₂O₃ seemed to maintain a relatively stable conversion with a conversion of 67% after 8 h. Noticeably, La₂O₃, as a promoter, only influences the stability of catalyst (not its activity). Furthermore, Al-Fatesh et al. (2014) previously demonstrated that La₂O₃, as a promoter, can accomplish a dual role in dry reforming reaction—it can restrict the disposition of carbon and reduce the acidity of the support. With that, the formation of pyrolytic carbon can be stopped since it favours the dissociation of CO₂. These characteristics accelerate the formation of carbon through the reverse Boudouard reaction (BR).

In contrast, CAT-2 recorded the highest conversion with an initial conversion of 88%. Besides that, the catalyst demonstrated prominent stability for 8 h. This can be associated with the properties of catalyst, as demonstrated by H₂-TPR (cf. Fig. 5) and CO₂-TPD (Fig. 6). Furthermore, CeO₂ is known as a promoter that facilitates or improves the dispersion of the active species on the surface of catalyst, as compared to the mono-oxides or bare support without the addition of promoter (Al-Swai et al., 2019). The coexistence of CeO₂ with other oxides increases the reducibility and oxygen storage capacity of the catalyst (Li and Gong, 2014). Damyanova et al. (2009) previously demonstrated that a slight amount of CeO₂ (e.g. 6 wt%) can stabilise the textural properties of the modified ZrO₂ having CeO₂.

Similarly, the conversion of CO₂, as shown in Fig. 7(b), appeared to exhibit the same trend as that of the conversion of CH₄. CAT-1 and CAT-3 recorded the same initial conversion of 83%. However, CAT-3 maintained a more stable conversion than CAT-1. Meanwhile, CAT-2 demonstrated the best conversion and stability but its conversion of CO₂ was higher than that of CH₄ due to the simultaneous generation of reverse water gas shift (RWGS) reaction (Dębek et al., 2016; Farooqi et al., 2020). Essentially, RWGS involves the reaction of CO₂ and H₂ to form CO. As shown in Fig. 6(c), the obtained results can be observed in terms of the molar ratio of H₂ and CO, where the ratio was found to be lower than 1 for CAT-1 (0.86), CAT-2 (0.95), and CAT-3 (0.89).

4. Conclusion

The performance of CAT-1, CAT-2, and CAT-3 were compared in the present study. The addition of CeO₂ as a promoter in Ni/Al₂O₃ catalyst appeared to improve the dispersion. Fur-

thermore, the obtained results on the performance of Ni/Al₂O₃-CeO₂ catalyst clearly reflected enhanced reducibility and basicity of catalyst through the active metal content on the surface of catalyst, where a higher and stable conversion was achieved. On the other hand, the addition of La₂O₃ in this study did not increase the conversion of the reactant but successfully maintained a relatively stable conversion over 8 h on stream. This may be due to the contribution of La₂O₃ in eliminating deposited carbon during the reaction. Besides that, the characterisation of fresh catalysts for FESEM characterisation revealed a homogeneous composition of catalysts for all samples. Nevertheless, CAT-3 yielded the best particle size and sharp FESEM image.

Declaration of Competing Interest

The authors declared that there is no conflict of interest.

Acknowledgement

The authors would like to thank Ministry of Education (MOE), Malaysia for providing financial assistance under FRGS/1/2018/TK02/UTP/02/10 and Universiti Teknologi PETRONAS for providing the required facilities to conduct this research work.

References

- Abd Ghani, N.A., Azapour, A., Syed Muhammad, A.F., Abdullah, B., 2019. Dry reforming of methane for hydrogen production over Ni-Co catalysts: Effect of Nb-Zr promoters. *Int. J. Hydrogen Energy* 44 (37), 20881–20888.
- Abdullah, B., Abd Ghani, N.A., Vo, D.V.N., 2017. Recent advances in dry reforming of methane over Ni-based catalysts. *J. Clean. Prod.* 162, 170–185.
- Aghamohammadi, S., Haghghi, M., Maleki, M., Rahemi, N., 2017. Sequential impregnation vs. sol-gel synthesized Ni/Al₂O₃-CeO₂ nanocatalyst for dry reforming of methane: Effect of synthesis method and support promotion. *Mol. Catal.* 431, 39–48.
- Al-Fatesh, A.S., Naeem, M.A., Fakeeha, A.H., Abasaed, A.E., 2014. Role of La₂O₃ as promoter and support in Ni/γ-Al₂O₃ catalysts for dry reforming of methane. *Chin. J. Chem. Eng.* 22, 28–37.
- Al-Swai, B.M., Osman, N., Alnarabiji, M.S., Adesina, A.A., Abdullah, B., 2019. Syngas production via methane dry reforming over ceria-magnesia mixed oxide-supported nickel catalysts. *Ind. Eng. Chem. Res.* 58, 539–552.
- Bartholomew, C.H., 2001. Mechanisms of catalyst deactivation. *Appl. Catal. A Gen.* 212, 17–60.
- Bian, Z., Das, S., Wai, M.H., Hongmanorom, P., Kawi, S., 2017. A review on bimetallic nickel-based catalysts for CO₂ reforming of methane. *ChemPhysChem* 18, 3117–3134.
- Bradford, M.C.J., Vannice, M.A., 1999. CO₂ reforming of CH₄. *Catal. Rev. – Sci. Eng.* 41, 1–42.
- Charisiou, N.D., Tzounis, L., Sebastian, V., Hinder, S.J., Baker, M.A., Polychronopoulou, K., Goula, M.A., 2019. Investigating the correlation between deactivation and the carbon deposited on the surface of Ni/Al₂O₃ and Ni/La₂O₃-Al₂O₃ catalysts during the biogas reforming reaction. *Appl. Surf. Sci.* 474, 42–56.
- da Fonseca, R.O., Rabelo-Neto, R.C., Simões, R.C.C., Mattos, L.V., Noronha, F.B., 2020. Pt supported on doped CeO₂/Al₂O₃ as catalyst for dry reforming of methane. *Int. J. Hydrogen Energy* 45, 5182–5191.
- Damyanova, S., Pawelec, B., Arishtirova, K., Huerta, M.V.M., Fierro, J.L.G., 2009. The effect of CeO₂ on the surface and catalytic

- properties of Pt/CeO₂-ZrO₂ catalysts for methane dry reforming. *Appl. Catal. B Environ.* 89, 149–159.
- De Freitas Silva, T., Dias, J.A.C., MacIel, C.G., Assaf, J.M., 2013. Ni/Al₂O₃ catalysts: Effects of the promoters Ce, La and Zr on the methane steam and oxidative reforming reactions. *Catal. Sci. Technol.* 3, 635–643.
- Dębek, R., Motak, M., Duraczyska, D., Launay, F., Galvez, M.E., Grzybek, T., Da Costa, P., 2016. Methane dry reforming over hydrothermalite-derived Ni-Mg-Al mixed oxides: The influence of Ni content on catalytic activity, selectivity and stability. *Catal. Sci. Technol.* 6, 6705–6715.
- Djinović, P., Batista, J., Pintar, A., 2012. Efficient catalytic abatement of greenhouse gases: Methane reforming with CO₂ using a novel and thermally stable Rh-CeO₂ catalyst. *Int. J. Hydrogen Energy* 37, 2699–2707.
- Donohue, M.D., Aranovich, G.L., 1998. Classification of Gibbs adsorption isotherms. *Adv. Colloid Interface Sci.* 76–77, 137–152.
- Farooqi, A.S., Al-Swai, B.M., Ruslan, F.H., Mohd Zabidi, N.A., Saidur, R., Syed Muhammad, S.A.F., Abdullah, B., 2020. Syngas production via dry reforming of methane over Ni based catalysts. *IOP Conf. Ser.: Mater. Sci. Eng.* 736, 42007.
- Fayaz, F., Danh, H.T., Ngyuen-Huy, C., Vu, K.B., Abdullah, B., Vo, D.V.N., 2016. Promotional Effect of Ce-dopant on Al₂O₃-supported Co Catalysts for Syngas Production via CO₂ Reforming of Ethanol. *Procedia Eng.* 148, 646–653.
- Ghoneim, S.A., El-Salamony, R.A., El-Temtamy, S.A., 2016. Review on innovative catalytic reforming of natural gas to syngas. *World J. Eng. Technol.* 04, 116–139.
- Guo, J., Lou, H., Zhao, H., Chai, D., Zheng, X., 2004. Dry reforming of methane over nickel catalysts supported on magnesium aluminate spinels. *Appl. Catal. A Gen.* 273, 75–82.
- Jang, W.J., Jeong, D.W., Shim, J.O., Roh, H.S., Son, I.H., Lee, S.J., 2013. H₂ and CO production over a stable Ni-MgO-Ce_{0.8}Zr_{0.2}O₂ catalyst from CO₂ reforming of CH₄. *Int. J. Hydrogen Energy* 38, 4508–4512.
- Jiang, P., Shang, Y., Cheng, T., Bi, Y., Shi, K., Wei, S., Xu, G., Zhen, K., 2003. Methane decomposition over Ni/ α -Al₂O₃ Promoted by La₂O₃ and CeO₂. *J. Nat. Gas Chem.* 12, 183–188.
- Kargbo, D.M., Wilhelm, R.G., Campbell, D.J., 2010. Natural gas plays in the marcellus shale: Challenges and potential opportunities. *Environ. Sci. Technol.* 44, 5679–5684.
- Kim, T.W., Park, J.C., Lim, T.H., Jung, H., Chun, D.H., Lee, H.T., Hong, S., Yang, J. II, 2015. The kinetics of steam methane reforming over a Ni/ γ -Al₂O₃ catalyst for the development of small stationary reformers. *Int. J. Hydrogen Energy* 40, 4512–4518.
- Le Saché, E., Santos, J.L., Smith, T.J., Centeno, M.A., Arellano-García, H., Odriozola, J.A., Reina, T.R., 2018. Multicomponent Ni-CeO₂ nanocatalysts for syngas production from CO₂/CH₄ mixtures. *J. CO₂ Util.* 25, 68–78.
- Li, S., Gong, J., 2014. Strategies for improving the performance and stability of Ni-based catalysts for reforming reactions. *Chem. Soc. Rev.* 43, 7245–7256.
- Luisetto, I., Tuti, S., Battocchio, C., Lo Mastro, S., Sodo, A., 2015. Ni/CeO₂-Al₂O₃ catalysts for the dry reforming of methane: The effect of CeAlO₃ content and nickel crystallite size on catalytic activity and coke resistance. *Appl. Catal. A Gen.* 500, 12–22.
- Mozammel, T., 2017. Catalyst development and process intensification towards syngas production through methane reforming.
- Nieva, M.A., Villaverde, M.M., Monzón, A., Garetto, T.F., Marchi, A.J., 2014. Steam-methane reforming at low temperature on nickel-based catalysts. *Chem. Eng. J.* 235, 158–166.
- Oyama, S.T., Hacırlıoğlu, P., Gu, Y., Lee, D., 2012. Dry reforming of methane has no future for hydrogen production: Comparison with steam reforming at high pressure in standard and membrane reactors. *Int. J. Hydrogen Energy* 37, 10444–10450.
- Penkova, A., Bobadilla, L., Ivanova, S., Domínguez, M.I., Romero-Sarria, F., Roger, A.C., Centeno, M.A., Odriozola, J.A., 2011. Hydrogen production by methanol steam reforming on NiSn/MgO-Al₂O₃ catalysts: The role of MgO addition. *Appl. Catal. A Gen.* 392, 184–191.
- Radlik, M., Adamowska-Teyssier, M., Krztoń, A., Koziel, K., Krajewski, W., Turek, W., Da Costa, P., 2015. Dry reforming of methane over Ni/Ce_{0.62}Zr_{0.38}O₂ catalysts: Effect of Ni loading on the catalytic activity and on H₂/CO production. *Comptes Rendus Chim.* 18, 1242–1249.
- Rahbar Shamskar, F., Rezaei, M., Meshkani, F., 2017. The influence of Ni loading on the activity and coke formation of ultrasound-assisted co-precipitated Ni-Al₂O₃ nanocatalyst in dry reforming of methane. *Int. J. Hydrogen Energy.* 42, 4155–4165.
- Selvarajah, K., Phuc, N.H.H., Abdullah, B., Alenazey, F., Vo, D.V.N., 2016. Syngas production from methane dry reforming over Ni/Al₂O₃ catalyst. *Res. Chem. Intermed.* 42, 269–288.
- Siang, T.J., Pham, T.L.M., Cuong, N. Van, Phuong, P.T.T., Phuc, N. H.H., Truong, Q.D., Vo, D.V.N., 2018a. Combined steam and CO₂ reforming of methane for syngas production over carbon-resistant boron-promoted Ni/SBA-15 catalysts. *Microporous Mesoporous Mater.* 262, 122–132.
- Siang, T.J., Singh, S., Omeregbe, O., Bach, L.G., Phuc, N.H.H., Vo, D.V.N., 2018b. Hydrogen production from CH₄ dry reforming over bimetallic Ni-Co/Al₂O₃ catalyst. *J. Energy Inst.* 91, 683–694.
- Stroud, T., Smith, T.J., Le Saché, E., Santos, J.L., Centeno, M.A., Arellano-García, H., Odriozola, J.A., Reina, T.R., 2018. Chemical CO₂ recycling via dry and bi reforming of methane using Ni-Sn/Al₂O₃ and Ni-Sn/CeO₂-Al₂O₃ catalysts. *Appl. Catal. B Environ.* 224, 125–135.
- Tao, W., Cheng, H., Yao, W., Lu, X., Zhu, Q., Li, G., Zhou, Z., 2014. Syngas production by CO₂ reforming of coke oven gas over Ni/La₂O₃-ZrO₂ catalysts. *Int. J. Hydrogen Energy* 39, 18650–18658.
- Usman, M., Wan Daud, W.M.A., Abbas, H.F., 2015. Dry reforming of methane: Influence of process parameters – A review. *Renew. Sustain. Energy Rev.* 45, 710–744.
- Wang, S., Lu, G.Q., Millar, G.J., 1996. Carbon dioxide reforming of methane to produce synthesis gas over metal-supported catalysts: State of the art. *Energy Fuels* 10, 896–904.
- Wang, Y., Yao, L., Wang, S., Mao, D., Hu, C., 2018a. Low-temperature catalytic CO₂ dry reforming of methane on Ni-based catalysts: A review. *Fuel Process. Technol.* 168, 199–206.
- Wang, Ye, Yao, L., Wang, Yannan, Wang, S., Zhao, Q., Mao, D., Hu, C., 2018b. Low-temperature catalytic CO₂ dry reforming of methane on Ni-Si/ZrO₂ catalyst. *ACS Catal.* 6, 6495–6506.
- Wu, H., La Parola, V., Pantaleo, G., Puleo, F.P., Venezia, A.M., Liotta, L.F., 2013. Ni-based catalysts for low temperature methane steam reforming: Recent results on Ni-Au and comparison with other bi-metallic systems. *Catalysts* 3, 563–583.
- Xu, G., Shi, K., Gao, Y., Xu, H., Wei, Y., 1999. Studies of reforming natural gas with carbon dioxide to produce synthesis gas. X. The role of CeO₂ and MgO promoters. *J. Mol. Catal. A: Chem.* 47–54.
- Xu, J., Zhou, W., Li, Z., Wang, J., Ma, J., 2009a. Biogas reforming for hydrogen production over nickel and cobalt bimetallic catalysts. *Int. J. Hydrogen Energy* 34, 6646–6654.
- Xu, J., Zhou, W., Wang, J., Li, Z., Ma, J., 2009b. Characterization and analysis of carbon deposited during the dry reforming of methane over Ni/La₂O₃/Al₂O₃ catalysts. *Cuihua Xuebao/Chin. J. Catal.* 30, 1076–1084.
- Xu, L., Wang, F., Chen, M., Yang, H., Nie, D., Qi, L., Lian, X., 2017. Alkaline-promoted Ni based ordered mesoporous catalysts with enhanced low-temperature catalytic activity toward CO₂ methanation. *RSC Adv.* 7, 18199–18210.
- Xu, X., Li, P., Shen, Y., 2013. Small-scale reforming of diesel and jet fuels to make hydrogen and syngas for fuel cells: A review. *Appl. Energy* 108, 202–217.
- Yao, L., Galvez, M.E., Hu, C., Da Costa, P., 2018. Synthesis gas production via dry reforming of methane over manganese promoted nickel/cerium-zirconium oxide catalyst. *Ind. Eng. Chem. Res.*

- Yao, L., Galvez, M.E., Hu, C., Da Costa, P., 2017. Mo-promoted Ni/Al₂O₃ catalyst for dry reforming of methane. *Int. J. Hydrogen Energy* 42, 23500–23507.
- Zhang, Z.L., Tspouriaris, V.A., Efstathiou, A.M., Verykios, X.E., 1996. Reforming of methane with carbon dioxide to synthesis gas over supported rhodium catalysts: I. Effects of support and metal crystallite size on reaction activity and deactivation characteristics. *J. Catal.* 158, 51–63.
- Zhao, Z., Ren, P., Li, W., Miao, B., 2017. Effect of mineralizers for preparing ZrO₂ support on the supported Ni catalyst for steam-CO₂ bi-reforming of methane. *Int. J. Hydrogen Energy* 42, 6598–6609.